Version of Record: https://www.sciencedirect.com/science/article/pii/S002231152030283X
Manuscript_a2d2f72b3df51c8f948e630f38425a65

Cluster Dynamics Modeling of Irradiation Growth in Single Crystal Zr

Yang Li and Nasr Ghoniem

Department of Mechanical and Aerospace Engineering, University of California Los Angeles, Los Angeles, CA, 90095, USA

Abstract

Irradiation growth of single-crystal Zr is modeled with a *reduced set* of cluster dynamics equations. Nucleation and growth of basal and prismatic dislocation loops are both accounted for in the model. Equations are developed for the time evolution of single point defects, a limited number of point defect clusters, interstitial and vacancy loop nucleation rates, as well as for the growth of vacancy loops on basal planes and interstitial loops on prismatic planes. Reduction of the usual infinite hierarchy of cluster dynamics equations to the simple set studied here is justified on the physical basis of the stability of small loops once nucleated. This simplified cluster dynamics model with a small number of adjustable parameters avoids the complexity of explicit representation of higher order point defect clusters. The model shows consistency with experimental observations of the following aspects: (1) The growth rates of Zr crystals along the a- and c-axes; (2) the onset dose for breakaway irradiation growth; (3) the saturation dislocation loop densities of vacancy and interstitial loops; (4) the effects of cold work and temperature on irradiation growth.

Keywords: zirconium, irradiation growth, cluster dynamics, dislocation loops, nucleation, growth

Email address: yangli0401@ucla.edu and nghoniem@gmail.com (Yang Li and Nasr Ghoniem)

1. Introduction

Irradiation growth is a phenomenon that describes dimensional changes without an applied stress. The phenomenon is found in irradiated HCP metals, especially zirconium, and is characterized by an expansion along the a-axis and contraction along the c-axis of hexagonal crystals. Experiments have shown that irradiation growth of annealed Zr crystals consists of three distinct stages [1]. Stage I exhibits a steep strain increase from ~ 0.1 to ~ 1 displacements per atom (dpa). Stage II displays a very low strain rate, often recognized as a strain plateau and lasts up to ~ 3 dpa. Stage III at high dose is referred to as the breakaway stage, accompanied with an accelerated growth strain rate. These different growth strain behaviors are believed to be strongly correlated with the formation and growth of both prismatic $\langle a \rangle$- and basal $\langle c \rangle$-dislocation loops. In cold-worked materials however, the strain rates are relatively high from the very beginning, and no strain plateau is formed [2, 3]. Irradiated Zr and its alloys develop a highly complex and dynamical defect microstructure, characterized by a mixture of mobile and sessile defects of both interstitial and vacancy types. The development of the defect network leads to a variety of changes in the macroscopic mechanical properties, including irradiation growth. The influence of such changes in the microstructure is generally deleterious, and is associated with a degradation in the longevity of the fuel cladding in Light Water Reactors (LWR), potentially compromising their safety. Experimental data for irradiation growth of Zr-based materials have been extensively summarized recently by Adamson [4].

A number of theoretical models have been developed to study the irradiation growth since the early 1960s, primarily based on a rate-theory approach (the reader is referred to more dedicated reviews [4–6]). Some early models assumed that only interstitial loops were formed during irradiation and growth occurred due to an excess of vacancies absorbed by grain boundaries [7, 8]. Transmission electron microscopy observations of irradiated Zr samples, however, revealed the co-existence of interstitial and vacancy-type $\langle a \rangle$-loops, and the formation of vacancy-type $\langle c \rangle$-loops [9]. A significant step in understanding irradiation growth was achieved by Woo and Gösele, who introduced the concept of intrinsic interstitial anisotropic diffusion, or known as the Diffusion Anisotropy Difference (DAD) [10, 11]. DAD provided a means of having variable bias differentials according to the orientation of the sinks, and thus explains the opposite defect flux

toward a- and c-axes, as well as the crucial role of $\langle c \rangle$-loops in the breakaway growth of annealed crystals. Another achievement was made by Holt et al. [12] by introducing the Production Bias Model (PBM). In the PBM, an attempt was made to account for differences in the production rates (hence bias) of cascade-induced interstitial and vacancy clusters.

Recent progress in modelling the irradiation growth based on the rate theory approach was achieved by Christien et al. [13], Choi et al. [14], and Barashev et al. [15]. By means of cluster dynamics accounting for the DAD concept, Christien et al. [13] have successfully reproduced the irradiation growth of single crystal zirconium. However, their model assumed that only point defects are mobile whereas all clustering defects are sessile. Such an assumption is not consistent with experiments and atomic simulation results, where small SIA clusters are highly mobile and migrate one-dimensionally along close-packed directions in Zr [16]. They also hypothesized that vacancy-type $\langle c \rangle$-loops nucleate on small iron clusters with an initial radius. Choi et al. [14] have then developed a mean-field rate theory based model. Incorporating the bias differentials for different sinks, the model has been extended to study the irradiation growth in polycrystal zirconium. Unfortunately, only point defects were considered in their model and c-axis growth strain was not shown. In contrast, Barashev et al. [15] proposed a reaction-diffusion model based on the PBM concept. Specifically, a-axis growth in their model was contributed from the 1D migrating SIA clusters. However, the interactions between different mobile species, such as the interstitial-vacancy recombination were neglected. In addition, their c-axis growth strain was two times larger than experimental data. More importantly, the nucleation rates of both $\langle a \rangle$- and $\langle c \rangle$-loops in two latter models were fitted rather than modeled for the sake of reproducing experimental results. A physical and detailed description on the loop nucleation and growth, as well as their influence on the irradiation growth is still missing. Under this circumstance, a cluster dynamics model with a *reduced set* of rate equations is developed, which accounts for the mobile point defects, the mobile SIA clusters and the nucleation and growth of interstitial and vacancy loops. The model specifically avoids heavy computations of brute force cluster dynamics with traditionally large numbers of Ordinary Differential Equations (ODEs), and large-scale Monte Carlo stochastic cluster dynamics simulations.

We first describe a proposed hybrid model that accounts for *both* nucleation and growth of dislocation loops in single-crystal Zr in the next

section, where key features associated with experimental observations of irradiation growth in Zr are summarized in subsection 2.1. The proposed cluster dynamics equations representing single point defects and their clusters are presented in subsection 2.2. Stages of dislocation loop nucleation and growth are discussed in subsection 2.3, and the experimental data and model parameters are given in subsection 2.4. Results of the model are then presented in section 3, where comparison with experimental data is given and the influence of key model parameters is discussed. Finally, a general discussion and conclusions of the study are presented in section 4.

2. Model Description

2.1. Irradiation Growth Mechanisms

Dislocation loops created by neutron radiation damage are the dominant source of irradiation growth in single crystal zirconium. These loops are either $\langle a \rangle$- or $\langle c \rangle$-dislocation loops, lying on the prismatic and basal planes, respectively [17–20]. Experimental observations have confirmed the co-existence of both perfect vacancy and interstitial type $\langle a \rangle$-loops with Burgers vector $\boldsymbol{b} = 1/3\langle 11\bar{2}0 \rangle$. The ratio of vacancy-to-interstitial loop density strongly depends on the irradiation temperature. By contrast, only vacancy-type $\langle c \rangle$-loops have been observed on the basal planes, which are either faulted with Burgers vector $\boldsymbol{b} = 1/2\langle 0001 \rangle$ and $\boldsymbol{b} = 1/6\langle 20\bar{2}3 \rangle$ or perfect with $\boldsymbol{b} = \langle 0001 \rangle$. Additionally, $\langle a \rangle$-dislocation loops are formed during stages I and II of irradiation, whereas $\langle c \rangle$-dislocation loops can be observed during stage III only, after an incubation dose of several displacements per atom (dpa).

Irradiation growth of Zr is then associated with the interaction between small radiation defects and nucleated dislocation loops. A large amount of point defects, i.e., vacancies and interstitials are generated during stage I. The migration energy of interstitials is much lower than their vacancy counterpart. The difference in the diffusivity of vacancies and interstitials and the bias due to elastic interaction with interstitials induces a net interstitial flux towards the $\langle a \rangle$-dislocation lines and loops lying on the prismatic plane, which results in an early expansion along $\langle a \rangle$ directions. This concept is well established in the Ball's work [21].

During the transient regime of early irradiation (below a few dpa), interstitials are continuously absorbed by various dislocation-type sinks until quasi-equilibrium is achieved. At this middle stage, the net flux of

point defects to interstitial loops decreases or is nearly to zero, which leads to the formation of a irradiation growth plateau. Although recent Molecular Dynamics (MD) simulations [22] show a new possible mechanism that the remaining vacancies agglomerate into $\langle a \rangle$-vacancy clusters during stage II and compensate the expansion due to $\langle a \rangle$-interstitial clusters, the basic idea remains the same – the dynamic balance between the vacancy and interstitial fluxes.

Along with the formation of $\langle a \rangle$- and $\langle c \rangle$-dislocation loops in prismatic and basal planes during stage III, there is a "bias" towards interstitials due to the elastic interaction between dislocations and point defects. This "bias" results in the net accumulation of interstitial or vacancy point defects at dislocation loop sinks with different orientations. The continuous growth of these loops finally results in what is known as "breakaway growth" behavior, where the growth rate is nearly constant.

For the sake of reproducing the aforementioned three stages of irradiation growth, a proposed model should be able to characterize the evolution of defect concentrations as a function of radiation dose, the nucleation of dislocation loops, and their subsequent growth. In addition, the model should consistently describe a wide range of experimental observations. In next section, a cluster dynamics model with limited rate equations is introduced.

2.2. Cluster Dynamics Equations

Four major microstructure features are taken into account in the present model. These are $\langle a \rangle$- and $\langle c \rangle$-edge dislocation lines, interstitial type $\langle a \rangle$-dislocation loops and vacancy type $\langle c \rangle$-dislocation loops. Assuming that the dislocation line density does not change during irradiation, dislocation loops grow or shrink by absorbing mobile defects. The total dislocation-type density of sinks for mobile defects is thus expressed as

$$\begin{aligned} \rho_{tot} &= \rho_d^a + \rho_d^c + \rho_{il}^a + \rho_{vl}^c \\ &= \rho_d^a + \rho_d^c + 2\pi r_{il}^a N_{il}^a + 2\pi r_{vl}^c N_{vl}^c \end{aligned} \tag{1}$$

where ρ_d^a and ρ_d^c are edge dislocation densities, and ρ_{il}^a and ρ_{vl}^c are interstitial and vacancy dislocation loop densities, with Burgers vectors along $\boldsymbol{a}$ and $\boldsymbol{c}$ directions, respectively. r_{il}^a and r_{vl}^c are the mean radii of interstitial and vacancy type loops, and N_{il}^a and N_{vl}^c are number densities of interstitial and vacancy type loops. Vacancy type $\langle a \rangle$ dislocation loops are not considered in this study.

The mean-field rate theory is based on the concept that all sinks are homogeneously distributed in space and that they receive an identical mobile defect flux [23–25]. Prismatic dislocations along the three equivalent directions $\boldsymbol{a1}$, $\boldsymbol{a2}$, and $\boldsymbol{a3}$ have three-fold symmetry as a result of hexagonal crystal symmetry, and are thus represented together as $\boldsymbol{a}$-dislocations. Moreover, vacancy- and interstitial-type prismatic loops of larger enough size have almost the same efficiency for absorbing mobile defects [6]. Hence, they cannot grow at the same time in the clusters dynamics framework. Neglecting vacancy loops on the prismatic plane would therefore not cause any problem. This rationale has been widely demonstrated by several investigators [13–15]. Additionally, recent MD simulations have further confirmed this assumption. It is revealed that the vacancy type $\langle a \rangle$ clusters are usually formed during stage II, and that they are quickly annihilated at high dose due to the bias diffusion of interstitials. According to MD simulation results [22], newly-generated vacancy loops during stage III are $\langle c \rangle$-component loops lying on the basal plane. Modelling the co-existence and growth of both vacancy- and interstitial-type prismatic loops is further discussed in section 3.3.

MD simulations have shown that the majority of defects produced in displacement cascades of Zr consists of point defects and small-size clusters containing several number of point defects [26]. The model developed in the current work therefore accounts for mobile point defects, mobile di-interstitial and tri-interstitial clusters, and sessile vacancy clusters lying on the basal plane as the primary damage in cascades. The generated point defects exhibit 3D isotropic diffusion in the lattice, while di-interstitials and tri-interstitials are considered as one-dimensional (1D) mobile Self-Interstitial Atom (SIA) clusters migrating along $\boldsymbol{a}$ directions [27]. The system then evolves due to reactions involving diffusion of mobile defects, and the nucleation and growth of both vacancy and interstitial loops. Interstitial clustering is assumed to result from diffusional migration of interstitial atoms, and these interstitial prismatic loops grow or shrink by interacting with point defects and mobile SIAs clusters. On the other hand, vacancy loop formation is taken to result from the athermal collapse of collision cascades [6, 28], and these vacancy basal loops can interact with point defects only, namely single interstitials and single vacancies.

The evolution of defect concentrations (per unit volume), C, of single vacancies (subscript v), single SIAs (i), di-interstitals ($2i$) and tri-interstitals ($3i$) is obtained from the following mass conservation rate equations

$$\frac{dC_v}{dt} = \frac{G^{NRT}}{\Omega}(1-\epsilon_v^{eff}) - R_{iv}C_vC_i - \rho_{tot}^v D_v C_v - \beta_{2i}^v C_v C_{2i} - \beta_{3i}^v C_v C_{3i} \tag{2}$$

$$\frac{dC_i}{dt} = \frac{G^{NRT}}{\Omega}(1-\epsilon_{2i}-\epsilon_{3i}) + \beta_{2i}^v C_v C_{2i} + 2\alpha_{2i}^i C_{2i} + \alpha_{3i}^i C_{3i} - R_{iv}C_vC_i - \rho_{tot}^i D_i C_i - 2\beta_{1i}^i C_i C_i - \beta_{2i}^i C_i C_{2i} - \beta_{3i}^i C_i C_{3i} \tag{3}$$

$$\frac{dC_{2i}}{dt} = \frac{G^{NRT}}{\Omega}\frac{\epsilon_{2i}}{2} + \beta_{1i}^i C_i C_i + \alpha_{3i}^i C_{3i} + \beta_{3i}^v C_v C_{3i} - k_{cl}^2 D_{2i} C_{2i} - \alpha_{2i}^i C_{2i} - \beta_{2i}^i C_i C_{2i} - \beta_{2i}^v C_v C_{2i} \tag{4}$$

$$\frac{dC_{3i}}{dt} = \frac{G^{NRT}}{\Omega}\frac{\epsilon_{3i}}{3} + \beta_{2i}^i C_i C_{2i} - k_{cl}^2 D_{3i} C_{3i} - \alpha_{3i}^i C_{3i} - \beta_{3i}^i C_i C_{3i} - \beta_{3i}^v C_v C_{3i} \tag{5}$$

where G^{NRT} is standard dose rate in dpa/s and Ω is the atomic volume. ϵ_{2i} and ϵ_{3i} are the fraction of SIAs produced in the form of mobile di-interstitial and tri-interstitial clusters. ϵ_v^{eff} is the effective fraction of vacancies produced in vacancy clusters, depending on the vacancy loop number density. $\rho_{tot}^j = \rho_d^a Z_{da}^j + \rho_d^c Z_{dc}^j + \rho_{il}^a Z_{il}^j + Q\rho_{vl}^c Z_{vl}^j$ is the effective total dislocation sink strength which accounts for the bias factor Z_k^j of point defects ($j = i, v$) for k-type of sinks ($k = da, dc, il, vl$). Moreover, Q is an effective absorption efficiency for vacancy loops that accounts for the limited absorption of stacking fault tetrahedra (SFTs) of single vacancies. D_j is the diffusion coefficient of j-type monomers ($j = i, v, 2i, 3i$). And $R_{iv} = 4\pi r_{iv}(D_i + D_v)$ is the recombination rate of point defects characterized by the recombination radius r_{iv} [13].

In Eqs. (2)-(5), β_{ni}^j represents the reaction frequency at which a n-size SIA cluster reacts with a point defect of type j, α_{ni}^i the interstitial emission frequency for a n-size SIA cluster. The reaction rate for spherical interstitial-interstitial aggregation is written as [29, 30]

$$\beta_{1i}^i = 4\pi(r_i + r_i)D_i \tag{6}$$

where $r_i = \left(\frac{3\Omega}{4\pi}\right)^{1/3}$ is the point defect radius. Discarding 1D-1D reactions between interstitial clusters, the reaction between 3D diffusing point defects and 1D migrating SIA clusters is decomposed into two parts:

$$\beta_{ni}^j = \beta_{ni}^{j(im)} + \beta_{ni(im)}^j \tag{7}$$

where $\beta_{ni}^{j(im)}$ is the reaction rate of 1-D migrating SIA cluster of size n interacting with an immobile point defect ($j = i, v$), and $\beta_{ni(im)}^{j}$ is the rate for a 3D diffusing point defect interacting with an immobile SIA cluster [30].

$$\begin{aligned} \beta_{ni}^{j(im)} &= (\pi r_{ni}^2)^2 D_{ni} C_j \\ \beta_{ni(im)}^{j} &= 2\pi r_{ni} D_j \end{aligned} \tag{8}$$

where $r_{ni} = \left(\frac{n\Omega}{\pi|\boldsymbol{b}^{\alpha}|}\right)^{1/2}$ is the radius of n-size SIA clusters. Next, because of the low probability of point defect emission from small-size interstitial clusters, we only consider the thermal dissociation of di-interstitials, while all larger clusters are thermally stable. The thermal dissociation rates are then given as [31]:

$$\begin{aligned} \alpha_{2i}^{i} &= \beta_{1i}^{i} \exp\left(-\frac{E_{2i}^{b}}{k_B T}\right) \\ \alpha_{ni}^{i} &= 0 \quad (n \geq 3) \end{aligned} \tag{9}$$

where E_{2i}^{b} is the binding energy of di-interstitials.

The positive terms in the right-hand sides (RHSs) of Eqs. (2)-(5) account for the production of point defects and SIA clusters, while the negative terms account for the loss due to their interaction and absorption. The sink strength for 1D migrating SIA clusters, k_{cl}^2 is then given by [15, 32, 33];

$$k_{cl}^2 = 2\left(\frac{\pi r_{cd}}{2}\right)^2 \left(\frac{\rho^a}{3}\right)^2 \tag{10}$$

where r_{cd} is the capture radius of dislocations and loops for mobile SIA clusters and $\rho^a = \rho_d^a + \rho_{il}^a$ is the density of the dislocations in the prismatic plane, including both dislocation lines and dislocation loops.

2.3. Nucleation & Growth of Sessile Loops

We turn our attention now to the development of nucleation rate equations for sessile vacancy and interstitial dislocation loops. It should be noted that not much is known about the nucleation of loops, especially on the basal planes. In this reduced cluster dynamics framework, the nucleation of these sessile loops takes place only if the net flux of the corresponding mobile defects is positive. Since 4-SIAs clusters are arranged in the form of perfect $\langle a \rangle$ loops, as seen in MD simulations [27], the critical

nucleus size for SIA loops is therefore taken as 4 interstitials. Although small clusters acquire high 1D mobility in MD simulations, the diffusivity of SIA clusters consistent with experimental observations is always much smaller [34]. This may be associated with the presence of atomic size traps (i.e. impurities). Moreover, it will be shown that the interstitial loop density reaches a quasi-steady state (i.e. slow variation with dose) in less than 10^{-2} dpa. Following references [28, 35, 36], all SIA clusters larger than four interstitials are thus considered as sessile loops over the long-time scale. For more details related to the assumptions that allow truncation of the cluster dynamics hierarchy, the reader is referred to our earlier works [36, 37]. On the other hand, the nucleation of vacancy $\langle c \rangle$ loops is characterized by collisional rather than diffusional atomistic events, as shown in [38]. Accordingly, the nucleation rate equations for interstitial and vacancy loops are given as:

$$\frac{dN_{il}^{a}}{dt} = \beta_{3i}^{i} C_i C_{3i} \tag{11}$$

$$\frac{dN_{vl}^{c}}{dt} = \frac{G^{NRT}\epsilon_v}{\pi r_{nucl}^2 |\boldsymbol{b}^c|}\left(1 - V_{cap}^{c} N_{vl}^{c}\right) \tag{12}$$

where r_{nucl} is a characteristic size for vacancy cluster nuclei. Based on atomistic simulations, the vacancy clusters generated in cascades consists only several vacancies and are generally immobile [26]. The characteristic radius of the loop nucleus is taken to be that of a tetra-vacancy, $r_{nucl} = r_{4v}$. ϵ_v is the fraction of vacancies produced in vacancy clusters within one free cascade, which holds the relation $\epsilon_v^{eff} = \epsilon_v\left(1 - V_{cap}^{c} N_{vl}^{c}\right)$. And the last term $\left(1 - V_{cap}^{c} N_{vl}^{c}\right)$ on the RHS of Eq. (12) accounts for the overlap effect of vacancy loops; $V_{cap}^{c} = 1/N_{max}^{c}$ being the effective loop volume for coalescence, and N_{max}^{c} is the saturation density of $\langle c \rangle$ vacancy loops. Note that a comprehensive dose-dependent nucleation description generally requires a large number of cluster dynamics equations, one for each cluster size. However, in next section we will show that the present *reduced cluster dynamics model* with a small number of rate equations can qualitatively reproduce all experimental observations, including the temperature dependence of the steady-state loop densities. It also shows a great capacity in emulating the irradiation growth of single crystal Zr, which is intimately related with the sink strength (or dislocation density) rather than solely the density of loops.

Then using the mean-size approximation, the sessile loop radii can be expressed in terms of the loop density and the total number of defects in the interstitial or vacancy type loops S_i^a and S_v^c

$$\left\langle (r_{il}^a)^2 \right\rangle \approx \langle r_{il}^a \rangle^2 = \frac{S_i^a}{\pi \left| \boldsymbol{b^a} \right| N_{il}^a} \tag{13}$$

$$\left\langle (r_{vl}^c)^2 \right\rangle \approx \langle r_{vl}^c \rangle^2 = \frac{S_v^c}{\pi \left| \boldsymbol{b^c} \right| N_{vl}^c} \tag{14}$$

where $\boldsymbol{b^a}$ and $\boldsymbol{b^c}$ are Burgers vectors along $\boldsymbol{a}$ and $\boldsymbol{c}$ directions. The growth and shrinkage of sessile loops are characterized by interstitial or vacancy absorption. The change rates of total numbers of defects (per atomic site) in the loops are therefore expressed as

$$\Omega^{-1} \dot{S}_i^a = -2\pi r_{il}^a N_{il}^a (Z_{il}^v D_v C_v - Z_{il}^i D_i C_i) + 2k_{ila}^2 D_{2i} C_{2i} + 3k_{ila}^2 D_{3i} C_{3i} \tag{15}$$

$$\Omega^{-1} \dot{S}_v^c = Q 2\pi r_{vl}^c N_{vl}^c (Z_{vl}^v D_v C_v - Z_{vl}^i D_i C_i) \tag{16}$$

The rate of change of interstitial loops comprises point defect absorption (first term) and the contribution from the 1-D migrating SIA clusters (second and third terms). The partial sink strengths k_{ila}^2 of sessile interstitial loops for these mobile clusters are given by [15, 32, 33]

$$k_{ila}^2 = 2\left(\frac{\pi r_{cd}}{2}\right)^2 \frac{\rho^a}{3} \frac{\rho_{il}^a}{3} \tag{17}$$

The factor 1/3 in the above equation means that SIA clusters interact with dislocations in the same migrating directions only, namely one of three $\boldsymbol{a}$ directions. We emphasize that Eq. (17) accounts for the interaction of mobile SIA clusters with sessile prismatic dislocation loops of the same Burgers vector only, excluding the absorption of di- and tri-interstitials by edge dislocations. Only in the case of low edge dislocation density where $\rho^a \approx \rho_{il}^a$, this partial sink strength is approximately equal to the total sink strength k_{cl}^2.

According to experimental observations, basal vacancy-type loops are formed at high dose only. And some recent atomistic simulations have revealed that the agglomeration of vacancies is in the form of stacking fault tetrahedra (SFTs) at low dose, which in turn collapse into vacancy loops

beyond a critical size/dose, resulting in a jump of binding energy for the last vacancy ($E^b_{SFT} \rightarrow E^b_{vl}$ in Fig. 11 of [39]). As expressed in Eq. 16, the growth rate of vacancy type loops is entirely ascribed to point defect absorption. In a bid to account for such vacancy loop formation mechanism and the discontinuous increase in the binding energy, a parameter Q characterizing the absorption efficiency of vacancy $\langle c \rangle$ loops is introduced hereof. In other words, if the size of the vacancy loop is smaller than a critical value, i.e. $r^c_{vl} < r_{crit}$, $Q = C_{st} < 1$ is adopted to represent the lower stability (smaller absorption efficiency) of the vacancy clusters. And if $r^c_{vl} \geq r_{crit}$, the vacancy clusters are considered as fully developed vacancy loops with the absorption efficiency $Q = 1$. It thus gives

$$Q = \begin{cases} C_{st} < 1 & r^c_{vl} < r_{crit} \\ 1 & r^c_{vl} \geq r_{crit} \end{cases} \tag{18}$$

where C_{st} can be estimated from the ratio of $\exp(-E^b_{vl}/k_BT)/\exp(-E^b_{SFT}/k_BT)$. More complicated expressions of Q for each cluster size can be implemented by using atomistic simulation results. In the next section, we will show that even this simple set could well reproduce the vacancy loop formation mechanism and that this parameter plays a key role in the onset of breakaway irradiation growth. Another way to understand this parameter is that it can be regarded as the fraction of $\langle c \rangle$ vacancy clusters. Some other MD simulations disclosed that the $\langle c \rangle$-component loops are energetically more favorable only if their radius is larger than a critical value $r^c_{vl} \geq r_{crit}$, and that $\langle a \rangle$ and $\langle c \rangle$ lack a dislocation character at low dose [22].

Finally the irradiation growth and shrinkage rates (axial inelastic strains along the $\boldsymbol{a}$ and $\boldsymbol{c}$ directions) can be obtained by computing the net number of SIAs accumulated by dislocations and sessile loops in different directions, which gives;

$$\begin{aligned} \Omega^{-1}\dot{\epsilon^a} = &- A^a\rho^a_{il}(Z^v_{il}D_vC_v - Z^i_{il}D_iC_i) - A^a\rho^a_d(Z^v_{da}D_vC_v - Z^i_{da}D_iC_i) \\ &+ 2A^ak^2_{cl}D_{2i}C_{2i} + 3A^ak^2_{cl}D_{3i}C_{3i} \end{aligned} \tag{19}$$

$$\Omega^{-1}\dot{\epsilon^c} = - A^cQ\rho^c_{vl}(Z^v_{vl}D_vC_v - Z^i_{vl}D_iC_i) - A^c\rho^c_d(Z^v_{dc}D_vC_v - Z^i_{dc}D_iC_i) \tag{20}$$

where ϵ^a and ϵ^c are the irradiation growth strain along $\boldsymbol{a}$ and $\boldsymbol{c}$ directions. A^a and A^c are the corresponding average strain factors for sinks lying in prismatic and basal planes, associated with the hexagonal structure of single crystal Zr. For more details, please refer to references [7, 14, 15, 40].

Note that unlike its counterpart in the $\boldsymbol{a}$ direction, the growth strain rate in $\boldsymbol{c}$ is only caused by the accumulation of single vacancies on the basal plane.

2.4. Parameters and Experimental Data

We consider here a comparison with experimental data and assessment of parameter sensitivity at a temperature of 553 K unless stated otherwise. The magnitude of the Burgers vectors for $\langle c \rangle$ loops is taken to be the same as $\langle a \rangle$ loops, where $|\boldsymbol{b}^c| = |\boldsymbol{b}^a| = 3.23 \times 10^{-8}$ cm [41]. A reference bias factor of unity is used for interstitials absorbed on $\langle a \rangle$ loops, $Z^i_{ila} = 1.0$, and for vacancies absorbed by edge dislocations and loops, $Z^v_{da}, Z^v_{dc}, Z^v_{ila}, Z^v_{vlc} = 1.0$ [6]. The displacement damage rate is taken from experiments, $G^{NRT} = 10^{-7}$ dpa/s [42–44]. Other parameters used in this work are summarized in Table 1. According to atomic simulations, the diffusivity of small 1D mobile SIA clusters is as high as that of single interstitials on the basal plane [27, 45]. Thus, the same pre-factor D_0 is used, for simplicity. Indeed, different diffusion coefficients for small SIA clusters would not significantly influence the final result of irradiation growth, since the flux of these clusters towards sinks is proportional to the flux of $D_{2i}C_{2i}$ or $D_{3i}C_{3i}$ (more details can be found in references [13, 15]).

Table 1: Model parameters used in the present calculations.

Definition	Symbol	Value	Reference/Comment
Di-interstitial binding energy	E^b_{2i}	1.42 eV	[27, 31]
Diffusion coefficient of single interstitials	D_i	$8.1882 \times 10^{-6} \exp\left(-\frac{0.1\text{eV}}{k_B T}\right)$ cm^2/s	[13, 14]
Diffusion coefficient of vacancy	D_v	$4.9639 \times 10^{-9} \exp\left(-\frac{0.9\text{eV}}{k_B T}\right)$ cm^2/s	[13, 14]
Recombination radius	r_{iv}	1.0×10^{-7} cm	[46]
Capture radius of prismatic loops for SIA clusters	r_{cd}	6.0×10^{-8} cm	[15, 32, 33]
Critical radius for $\langle c \rangle$ loops	r_{crit}	4.0×10^{-7} cm	[22, 39]
Density of $\langle a \rangle$ dislocations	ρ^a_d	Single crystal: 7.25×10^6 cm^{-2}	[14, 44]
Density of $\langle c \rangle$ dislocations	ρ^c_d	Single crystal: 2.25×10^6 cm^{-2}	[14, 44]
Bias factor of interstitials for $\langle a \rangle$ dislocations	Z^i_{da}	1.56	[11, 14]
Bias factor of interstitials for $\langle c \rangle$ dislocations and loops	Z^i_{dc}, Z^i_{vlc}	0.586	[11, 14]
Average strain factor in $\langle a \rangle$ direction	A^a	0.5	[7]
Average strain factor in $\langle c \rangle$ direction	A^c	1.0	[7]
Diffusion coefficient of small SIA clusters	D_{2i}, D_{3i}	$8.1882 \times 10^{-6} \exp\left(-\frac{0.04\text{eV}}{k_B T}\right)$ cm^2/s	E^m_{ni} from [45]
Absorption efficiency for $\langle c \rangle$ loops	Q	0.2 ($r_{vc} < r_{crit}$)	Assumed
Fraction of interstitials produced as SIA clusters	$\epsilon_{2i}, \epsilon_{3i}$	3.5×10^{-4}	Assumed
Fraction of vacancies produced as clusters	ϵ_v	3.3×10^{-8}	Assumed
Saturation density of $\langle c \rangle$ loops	N^c_{max}	4×10^{14} cm^{-3}	Assumed

The last four assumed parameters are calibrated by matching the steady-state loop density determined by the nucleation rate equations (Eqs. (11)-(12)) to experimental data. It is worth to note that these four parameters

are sensitive to radiation conditions, e.g. the dose rate and the radiation temperature. Further discussion of these parameters could be found in section 3.3. Qualitative radiation-induced loop information has been described in section 2.1. Available quantitative experimental data for irradiated pure Zr are summarised in Table 2.

Table 2: Experimental data of radiation induced dislocation loops in pure Zr.

Irradiation source	Temperature	Particle fluence	Loop density	Mean size	Ref.
Zr ($E_{neutron} > 1$MeV)	300 °C	3.8×10^{23} m^{-2}	1.2×10^{22} m^{-3}	9 nm	[47]
		1.1×10^{25} m^{-2}	5.0×10^{21} m^{-3}	18.6 nm	[48]
	350 °C	2.0×10^{23} m^{-2}	8.0×10^{20} m^{-3}	< 10 nm	[47]
		5.3×10^{23} m^{-2}	2.7×10^{21} m^{-3}	23 nm	[47]
	400 °C	3.3×10^{23} m^{-2}	7.0×10^{20} m^{-3}	33 nm	[49]
		1.0×10^{25} m^{-2}	8.5×10^{20} m^{-3}	54 nm	[17]
	450 °C	1.3×10^{25} m^{-2}	1.0×10^{18} m^{-3}	–	[50]
Zr ($E_{Zr^+} = 0.5$MeV)	400 °C	1.26×10^{18} m^{-2}	2.3×10^{22} m^{-3}	6.9 nm	[51]
	450 °C	1.26×10^{18} m^{-2}	1.6×10^{22} m^{-3}	10.5 nm	[51]
	450 °C (+)[1]	1.26×10^{18} m^{-2}	1.4×10^{21} m^{-3}	19.9 nm	[51]
Zr ($E_{e^-} = 1$MeV)	450 °C	1.8×10^{25} m^{-2}	7.0×10^{20} m^{-3}	–	[51]
		2.8×10^{25} m^{-2}	8.1×10^{20} m^{-3}	–	[51]
		3.6×10^{25} m^{-2}	8.0×10^{20} m^{-3}	–	[51]
	500 °C	2.8×10^{25} m^{-2}	4.1×10^{20} m^{-3}	–	[51]
		3.6×10^{25} m^{-2}	4.5×10^{20} m^{-3}	–	[51]
	600 °C	4.6×10^{24} m^{-2}	0.9×10^{20} m^{-3}	–	[51]
		3.6×10^{25} m^{-2}	1.1×10^{20} m^{-3}	–	[51]

[1] (+): After annealing treatments.

It is obvious that the loop density and mean radius show high sensitivity to the irradiation source and conditions. At the same conditions, and compared to the neutron source, radiation by self-ions causes much higher loop density, whereas a contrary trend is found for electron irradiation. Whatever the irradiation source, increasing the radiation temperature generally induces a decrease in the loop density but a larger loop size. In summary, the total density of dislocation loops ranges from 10^{20} to 10^{22} m^{-3}, depending on the irradiation source, dose and temperature. Moreover, most the loop population is $\langle a \rangle$-component loops, which nucleate from the very beginning of irradiation. However, $\langle c \rangle$ vacancy loops do not appear to nucleate prior to a dose of $\sim$ 3 dpa, and magnitude of their density is generally one order of magnitude smaller than $\langle a \rangle$ loops. In the next section, we will show that this incubation dose for vacancy loops

can be naturally reproduced by introducing the absorption efficiency Q for $\langle c \rangle$ vacancy loops. Combining with the results reported in [6, 14, 52], the density of $\langle a \rangle$ interstitial loops N_{il}^{a}(dose = 0.1 dpa) $\sim 10^{21}$ m^{-3} and $\langle c \rangle$ vacancy loops N_{vl}^{c}(dose = 4.0 dpa) $\sim N_{max}^{c}$($\sim 10^{20}$ m^{-3}) are used to calibrate our assumed parameters. The corresponding evolution of the density of loops is presented in the following section.

3. Results

All rate equations in section 2 are solved using a Matlab ODE solver for stiff ODEs [53]. The results for single crystal Zr are examined in terms of defect concentrations, dislocation loop density, loop mean radius, and the irradiation growth strain components. The effect of the absorption efficiency Q on irradiation growth will be further examined. Finally, the irradiation growth strain of cold-worked zirconium and its temperature-dependency are evaluated and compared with available experimental data.

3.1. Single Crystal Zr with Low Dislocation Density

Defect concentrations display typical low-sink-density behavior in single crystal zirconium, as shown in Fig. 1. Initially, the concentrations increase because of the low reaction probability of defect recombination or interaction. Then, due to the high diffusivity of interstitials and small SIA clusters, the concentrations of single, di- and tri-interstitials begin to decrease, whereas the vacancy concentration increases at around 10^{-8} dpa. More interestingly, the concentrations of di- and and tri-interstitials both present fluctuations in the range of $10^{-8} - 10^{-4}$ dpa. This behavior indicates the nucleation of interstitial loops, and therefore the sink density continuously increases by absorbing more interstitials and SIA clusters. Finally, the concentrations of all defect types reach a steady state at around 0.5 dpa, which means that defect production is compensated by their loss to sinks.

Fig. 2a shows the evolution of the loop density using the model described in section 2.3. It is seen that for interstitial $\langle a \rangle$ loops, the loop density steeply increases due to the high diffusivity of single interstitial and SIA clusters, and then achieves a quasi steady-state value beyond $\sim$ 0.5 dpa. It is noted that the defect concentrations change very slowly at high dose. By contrast, the vacancy loops are formed only after $\sim$ 0.3 dpa, where the net vacancy flux towards $\langle c \rangle$ loops becomes positive. As described in section 2.1, the interstitial fluxes towards $\langle a \rangle$ and $\langle c \rangle$ directions are both

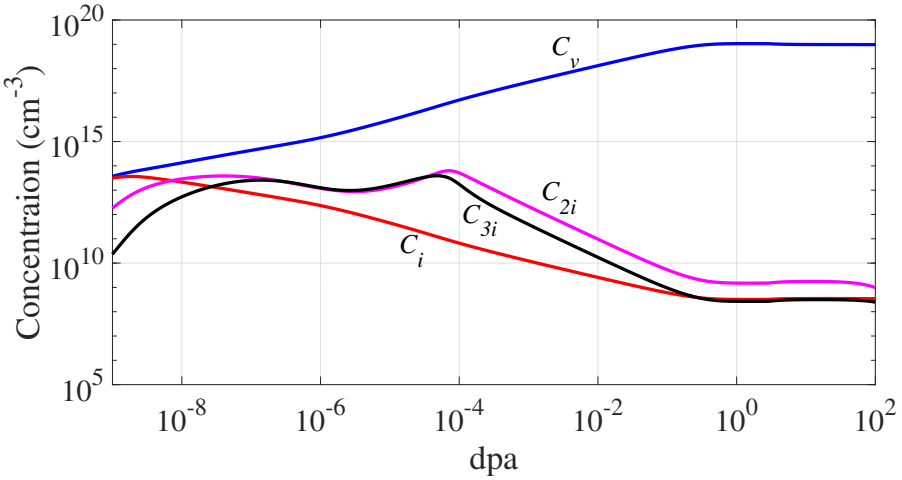

Figure 1: Concentrations of point defects, di-interstitials and tri-interstitials in single crystal zirconium at 553 K.

positive at stage I due to the high diffusivity of intersitititials. Hence, there is no surviving vacancy clusters at very low dose. This result is consistent with MD simulations [22]. Lastly, the density of vacancy loops reaches the final N^c_{max} around ~ 4 dpa. It is noted that the distribution of loop density with different sizes was given by Christien et al. at some discrete doses using cluster dynamics [13]. It is also seen that the density of small size clusters remains nearly constant beyond ~ 0.3 dpa, while the density of large clusters continues to increase. Unfortunately, the dose-dependency of loop density was not presented in their work. Therefore, it remains a considerable challenge to bring the loop nucleation mechanisms on par with atomistic simulations.

The dose dependence of interstitial and vacancy loop average radii is shown in Fig. 2b. First, the obtained value of ~ 10 nm is in good agreement with the experimentally observed radius for interstitial $\langle a \rangle$ loops at low dose [18, 19]. For vacancy $\langle c \rangle$ loops, a much larger value is obtained at high dose, which again correlates well with experimental observations. Moreover, the effect of the absorption efficiency Q for vacancy $\langle c \rangle$ loops is distinct, that is the change of the increase in slops at 3 dpa. It means that at lower dose (< 3 dpa), vacancy clusters with small radius are in the form of SFTs rather than fully-developed real loops. This may thus explain why vacancy $\langle c \rangle$ loops are never observed at low dose irradiation. It is also

worth noting that even with such a simplified nucleation model, similar evolution of the loop radii is obtained and compares well with full-fledged cluster dynamics simulations (Fig. 12 of [13]).

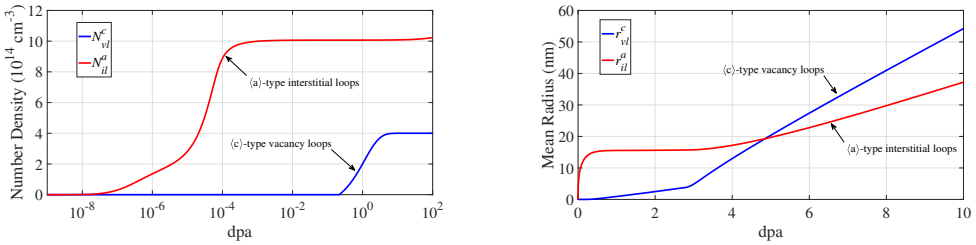

Figure 2: (a) density, and (b) mean loop radius of interstitial and vacancy loops in single crystal zirconium at 553 K.

Next, the calculated irradiation growth of single crystal zirconium is compared to experimental measurements for both iodide and zone refined crystals, and shown in Fig. 3. The $\langle a \rangle$-axis growth strain is in excellent agreement with experimental data for all three stages. The experimental values of the $\langle c \rangle$-axis shrinkage is higher than the calculations at the early irradiation stages I and II. This discrepancy at lower dose may be explained as follows. First, atomistic simulations indicate that SIA clusters on the prismatic plane will cause a shrinkage of the lattice in the $\boldsymbol{c}$-direction and therefore results in the $\langle c \rangle$-axis contraction. Second, other vacancy type defects, for instance bubbles and small nano-voids are not considered in this model, and may result in $\langle c \rangle$-axis contraction at low dose. Finally, the volume change due to the collapse of the SFTs, which takes place at a dose below $\sim$ 3 dpa, is not taken into account in the present model. It is also important to note that the onset dose $\sim$ 3 dpa for the breakaway growth is intrinsically reproduced by our model, rather than setting an incubation dose for vacancy loop nucleation.

For single crystal zirconium with lower initial dislocation density, the major contribution to irradiation growth is from the nucleation and growth of dislocation loops. The results are therefore determined by the properties of these loops, in terms of the defect flux and the dislocation density. Under this circumstance, the absorption efficiency Q plays an important role in our model. In the following, the effect of this parameter is investigated.

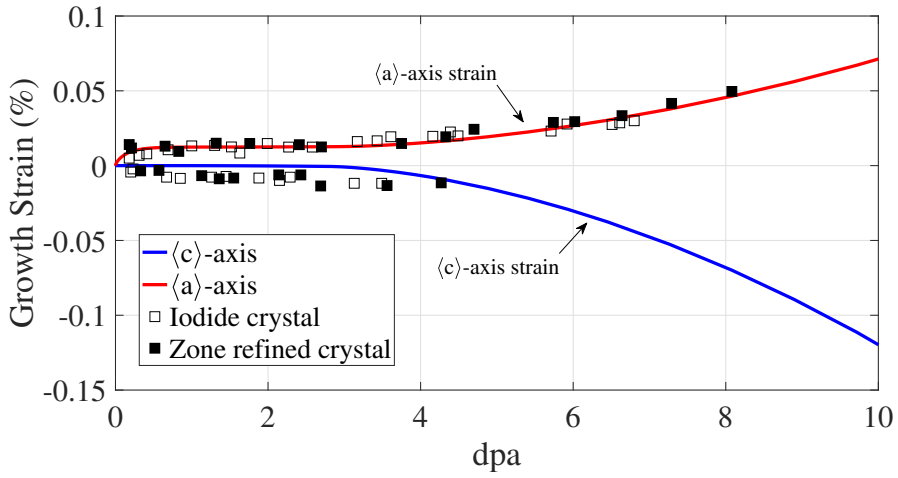

Figure 3: Comparison of the calculated growth strain with experimental measurements in single crystal zirconium at 553 K. Closed and open squares are for iodide and zone-refined purity zirconium [44], respectively.

It is noted that the nucleation of interstitial and vacancy loops is almost independent of this parameter Q. The loop density with different absorption efficiency remains the same as the previous case (Fig. 2a). Next, the loop radius evolution for two extreme conditions with $Q = 1$ and $Q = 0$ are presented in Fig. 4. $Q = 0$ means that the vacancy loops can not absorb any mobile defects, therefore the loop radius for vacancy loops remains zero throughout the simulation. After a dramatic increase during the transient stage, interstitial $\langle a \rangle$ loops can no longer grow due to the considerable remaining vacancies. On the other hand, for the case $Q = 1$, the radii of $\langle a \rangle$ and $\langle c \rangle$ loops keep on increasing at a steady-rate.

The corresponding irradiation growths are shown in Fig. 5 and compared to the experimental data, as well as the case $Q = 0.2$. For the case $Q = 0$, no breakaway behavior is observed. And for the case $Q = 1$, the breakaway stage subsequently follows the stage I. It is therefore obvious that higher parameter Q induces stronger breakaway growth. In conclusion, the absorption efficiency, or the formation of the real vacancy loops is responsible for the breakaway behavior of single crystal Zr. Similar results were obtained by Christien et al. [13]. In their model, pre-existing iron clusters were assumed to be the nucleation sites for vacancy clusters. In our approach, the onset dose of breakaway irradiation growth is correlated

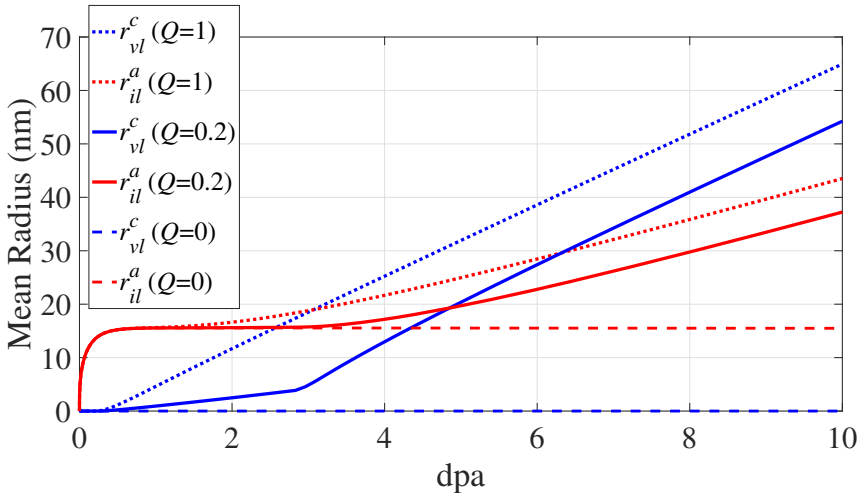

Figure 4: Effect of the absorption efficiency Q on the mean interstitial and vacancy loop radii.

with the formation of vacancy loops rather than their density [6, 11].

3.2. *Effect of Cold Work and Irradiation Temperature*

In cold worked crystals, dislocation lines become the dominant sinks for mobile defects, and the irradiation growth strain becomes nearly linearly dependent on the dose [3, 44, 54]. Accordingly, we can directly estimate the growth strain rate at the steady state of the system, where $\rho^a_d + \rho^c_d \gg \rho^a_{il} + \rho^a_{vl}$. Omitting the production of the vacancy and interstitial clusters, solution to the rate equations gives

$$D_v C_v \approx \frac{G^{NRT}/\Omega - R_{iv} C_i C_v}{Z^v_{da}\rho^a_d + Z^v_{dc}\rho^c_d} \tag{21}$$

$$D_i C_i \approx \frac{G^{NRT}/\Omega - R_{iv} C_i C_v}{Z^i_{da}\rho^a_d + Z^i_{dc}\rho^c_d} \tag{22}$$

Substituting Eqs. (21)-(22) in Eqs. (19)-(20) yields;

$$\dot{\epsilon}^a \approx -A^a (G^{NRT} - \Omega R_{iv} C_i C_v)\left(\frac{Z^v_{da}\rho^a_d}{Z^v_{da}\rho^a_d + Z^v_{dc}\rho^c_d} - \frac{Z^i_{da}\rho^a_d}{Z^i_{da}\rho^a_d + Z^i_{dc}\rho^c_d}\right) \tag{23}$$

$$\dot{\epsilon}^c \approx -A^c (G^{NRT} - \Omega R_{iv} C_i C_v)\left(\frac{Z^v_{dc}\rho^c_d}{Z^v_{da}\rho^a_d + Z^v_{dc}\rho^c_d} - \frac{Z^i_{dc}\rho^c_d}{Z^i_{da}\rho^a_d + Z^i_{dc}\rho^c_d}\right) \tag{24}$$

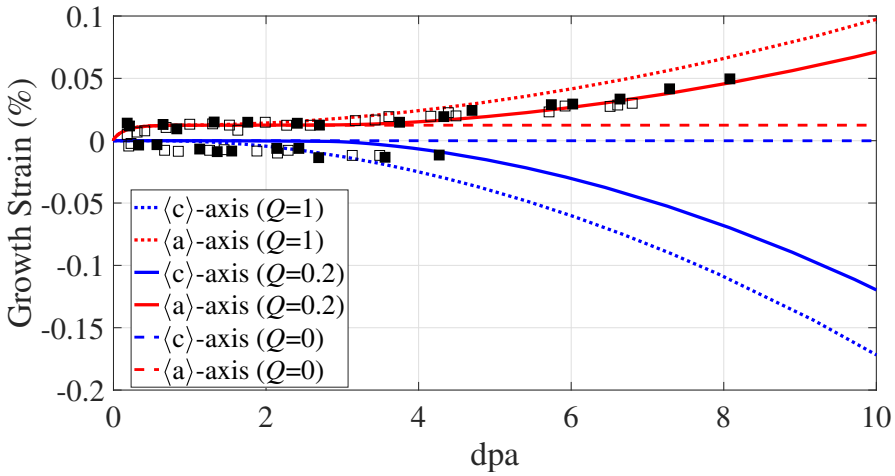

Figure 5: Effect of the absorption efficiency Q on irradiation growth.

Hence, in cold-worked materials, the growth strain rates depend only on the dislocation densities and defect generation and recombination rates. Taking the dislocation density $\rho_d^a + \rho_d^c \sim 10^{10}$ cm^{-2}, calculated defect concentrations show typical high-sink density behavior, as shown in Fig. 6. Compared to single-crystal zirconium of low dislocation density, defect concentrations reach the steady-state at lower dose, around 10^{-2} dpa. In addition, transients in SIA cluster concentrations, namely the nucleation of interstitial loops, are not observed because defects are primarily absorbed by dislocation lines. These results are consistent with the fact that dislocation lines in cold-worked materials are dominant, and hence it is difficult to form new dislocation loops in a material with saturated dislocation density.

Fig. 7 presents the corresponding irradiation growth in cold-worked zirconium at 553 K. The a-axis growth strain obtained from the simulation (solid line) and the approximate analysis of Eq. (23) (dashed line) are compared with the experimental results of 25% cold-worked zircaloy (closed circles) [44]. The fitted dislocation line density of $\sim 10^{14}$ m^{-2} agrees well with experimental measurements [44]. Moreover, the irradiation growth of cold-worked zirconium is accurately predicted by Eq. (23). It is obvious that an increase of the dislocation densities by an order of magnitude results in a steep linear dependence of growth strain on dose, with a slope of $\sim 10^{-3}$ dpa^{-1}. Note that the growth strain is about ~ 10 times larger than

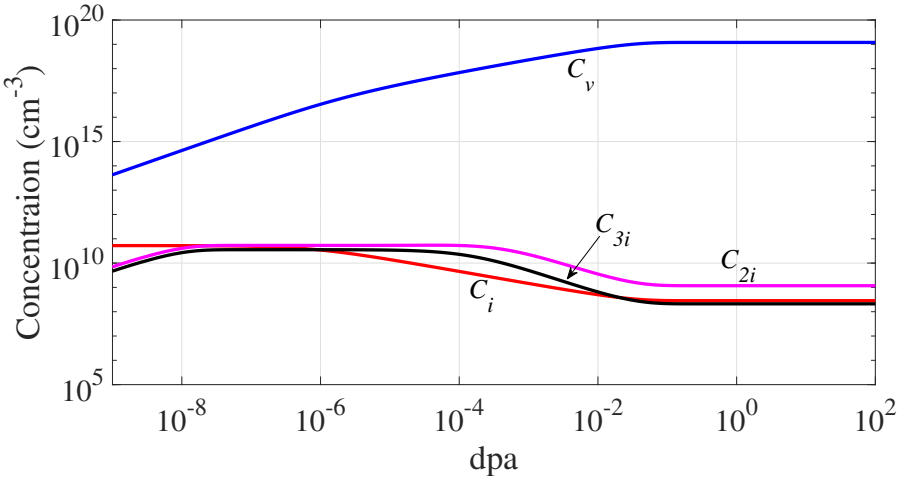

Figure 6: Defect concentrations in cold-worked zirconium at 553 K.

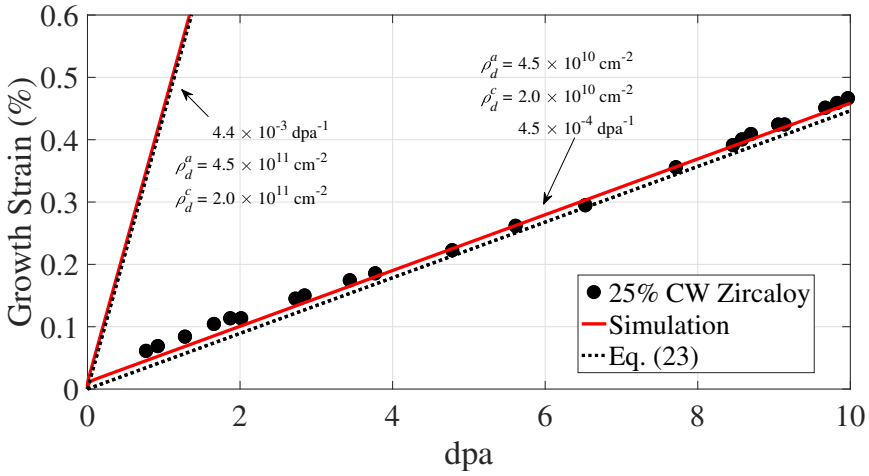

Figure 7: Irradiation growth in cold-worked zirconium at 553 K. Experimental results of 25% cold-worked (CW) zircaloy are from [44].

what is observed in single crystal Zr with low dislocation density. This is again in agreement with the maximum value observed for swaged Zr crystals [54].

Next, the effect of temperature on irradiation growth is examined. In the current model, several parameters are temperature-dependent, includ-

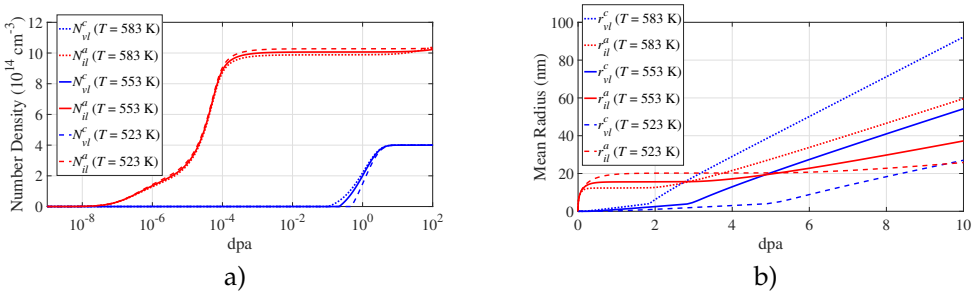

Figure 8: Effect of the irradiation temperature on the (a) density, and (b) mean loop radius, of interstitial and vacancy loops in single crystal zirconium.

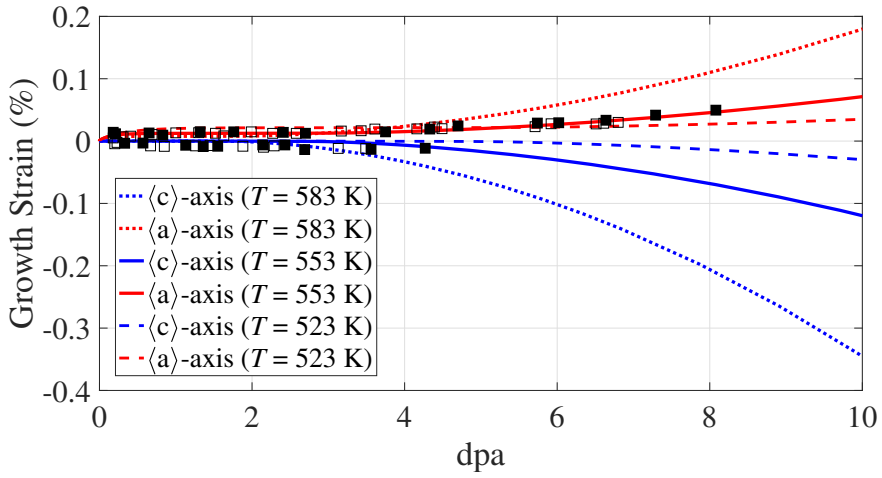

Figure 9: Effect of temperature T on irradiation growth.

ing the diffusion coefficients and the reaction rates of various species. Therefore small temperature variations (ΔT = 30 K) are considered on the premise that other parameters remains unchanged. Fig. 8 shows the loop density and mean radius of interstitial and vacancy loops at different irradiation temperatures. Globally, the experimentally observed irradiation temperature effect is successfully reproduced using the current nucleation model, where a higher temperature results in a lower loop density and a larger loop size. Particularly, an increase in the irradiation temperature favors the nucleation of vacancy $\langle c \rangle$ loops due to the higher diffusivity of mobile defects, which is also consistent with experimental observations

[55].

Fig. 9 shows the temperature effect on irradiation growth. The trend is consistent with experiments, where a higher temperature leads to stronger breakaway growth (see Fig. 3-26 in reference [4]). It again demonstrates that the irradiation growth is intimately related to the formation of $\langle c \rangle$-component vacancy loops on the basal plane.

However, the temperature effect on irradiation growth of Zr-based materials has been rarely modeled due to its complexity. Numerous factors are generally involved, including chemical compositions, manufacturing processes, microstructure, and so on. For instance, polycrystal zircaloy exhibits the opposite temperature dependency below and above $\sim$ 580 K [56], which appears to be associated with the temperature effect on DAD. A detailed description on the temperature effect therefore requires further efforts on understanding the loop nucleation mechanism and the sink strength under different conditions.

3.3. Discussions

Due to the lack of experimental data for irradiation growth of single crystal zirconium [4], all above calculations are performed for a given radiation condition with four free parameters, i.e. given dose rate and temperature. We therefore discuss the feasibility of modelling irradiation growth under different radiation conditions using this reduced cluster dynamics model hereafter. Indeed, the basis of irradiation growth in annealed zirconium is the nucleation and growth of interstitial and vacancy loops as described in section 2.1. Consequently, if the dose-dependent evolution of the loop number density and loop size can be reproduced for a given irradiation condition, it would naturally give rise to the accurate growth strain. As shown in the previous section, the temperature-dependent evolution of radiation-induced loop density and size is in qualitative agreement with experimental observations even without adjustment of the four free parameters. It is thus believed that the developed model in this work is applicable to a wide range of irradiation conditions. However, in light of MD simulation results of displacement cascades in metals, the four free parameters introduced in the current model should be taken as function of dose rate and radiation temperature [26, 57, 58]. Hence, in order to ultimately achieve quantitative prediction of irradiation growth in any other conditions, an alternate approach would be needed by fitting functions of these parameters to reproduce defect evolution obtained from full cluster

dynamics models. Moreover, it should be also pointed out that fractions of interstitials and vacancies produced in clusters used in this work are much smaller when compared to MD simulation results. This disparity may be caused by the over-estimated bias factors of dislocation loops for mobile defects and the uncertain nucleation mechanisms for dislocation loops, particularly for vacancy loops. It is therefore worth to review the bias factors in Zr and to establish a more comprehensive nucleation model with the aid of theoretical analysis and atomistic simulations.

Another challenge encountered with cluster dynamics modelling of irradiation growth in Zr is the incorporation of vacancy-type prismatic loops. Recent literature shows two primary rate-theory models describing irradiation growth in zirconium, i.e. DAD-based [11, 13, 14] and PBM-based [12, 33] models. These models are endowed with different pros and cons vis-a-vis modeling irradiation growth, but neither one can fully reproduce experimental observations. For DAD based models, irradiation growth is the result of the biased diffusion of point defects and the bias differential of various sinks [11, 13, 14]. Prismatic-type sinks preferably absorb interstitials, while basal-type defects are generally preferable sinks for vacancies. This bias difference always leads to a positive flux of interstitials towards prismatic directions. Hence, only interstitial-type loops can survive on prismatic planes in this framework. On the other hand, for PBM based models, defect clusters play a crucial role in irradiation growth [12, 33]. Although the presence of vacancy-type $\langle a \rangle$ loops in one of three prismatic directions have been successfully emulated in this type of models by using anisotropic initial conditions along the a-axes [15], neglecting the bias differential of sinks induces a fast annihilation of all vacancy prismatic loops at very low dose. Recent Monte Carlo calculations [59], which take into account the large vacancy and interstitial clusters created inside the cascade and the bias absorption of sinks, have demonstrated the simultaneous growth of both vacancy and interstitial loops at a dose of $\sim$ 0.1 dpa. Stochastic cluster dynamics accounting for the DAD and PBM concepts may be an appropriate alternative to ultimately demonstrate the co-existence and growth of vacancy and interstitial prismatic loops.

Lastly, interstitial prismatic loops associated with the a-axis growth always pose less problems compared with basal loops. According to atomistic simulations, stable SFTs, faulted $\langle c \rangle$-loops, perfect $\langle c \rangle$-loops and $\langle c+a \rangle$-loops are all observed using different potential energies [22, 39, 60–62]. A slight anisotropic diffusivity variation of vacancies will strongly influence

their clustering behavior [63]. It has been shown that the nucleation of the basal loops directly affects the breakaway growth of annealed zirconium. Further efforts are therefore needed for the sake of better understanding and modelling of vacancy loop nucleation.

The model developed in this work is an attempt to couple loop nucleation in a simple way to DAD and PBM ideas. It thus sheds light on the full development of cluster dynamics, which can account for DAD, one-dimensional migrating clusters (PBM), as well as a more physical nucleation theory for both interstitial and vacancy loops.

4. Conclusions

Irradiation growth of single-crystal zirconium is modeled with a *reduced set* of cluster dynamics equations, accounting for the simultaneous nucleation and growth of dislocation loops. Nucleation of interstitial-type prismatic loops and vacancy-type basal loops is clearly described for in the model, together with consideration of the sessile loop growth behavior, based on the mean-size approximation. A small number of parameters (on the order of four parameters) is fitted to available experimental data. The resultant evolution of the loop density is consistent with experimental observations. Moreover, the calculations reproduce the observed irradiation growth stages, including the growth rate along a- and c-axes, the onset dose for breakaway growth, the effects of cold work, and the influence of temperature. The crucial role of basal loops has been examined by varying the absorption efficiency of vacancy loops. It is confirmed that the onset dose for breakaway growth is determined by the formation of vacancy-type basal loops. Finally, the effects of cold work and temperature on irradiation growth are investigated, which are both in agreement with experimental observations. The current study is therefore an important step towards the full development of rate-theory based models for irradiation growth in zirconium.

Acknowledgments

This material is based upon work supported by the U.S. Department of Energy, Office of Science, Office of Fusion Energy Sciences, under Award Number DE-SC0018410 with UCLA. Discussions with Professor Jaime Marian (UCLA) are greatly acknowledged.

Data Availability

The raw/processed data required to reproduce these findings are available upon request from the authors.

References

[1] R. Holt, Mechanisms of irradiation growth of alpha-zirconium alloys, Journal of Nuclear Materials 159 (1988) 310–338.

[2] R. Zee, G. Carpenter, A. Rogerson, J. Watters, Irradiation growth in deformed zirconium, Journal of Nuclear Materials 150 (3) (1987) 319–330.

[3] S. I. Choi, J. H. Kim, Radiation-induced dislocation and growth behavior of zirconium and zirconium alloys – A review, Nuclear Engineering and Technology 45 (3) (2013) 385–392. doi:10.5516/NET.07.2013.035.

[4] R. B. Adamson, C. E. Coleman, M. Griffiths, Irradiation creep and growth of zirconium alloys: A critical review, Journal of Nuclear Materials 521 (2019) 167–244. doi:10.1016/j.jnucmat.2019.04.021.

[5] R. A. Holt, In-reactor deformation of cold-worked Zr–2.5Nb pressure tubes, Journal of Nuclear Materials 372 (2) (2008) 182–214. doi:10.1016/j.jnucmat.2007.02.017.

[6] F. Onimus, J. Béchade, Radiation Effects in Zirconium Alloys, in: Comprehensive Nuclear Materials, Elsevier, 2012, pp. 1–31. doi:10.1016/B978-0-08-056033-5.00064-1.

[7] C. Dollins, In-pile dimensional changes in neutron irradiated zirconium base alloys, Journal of Nuclear Materials 59 (1) (1976) 61–76.

[8] D. Fainstein-Pedraza, E. Savino, A. Pedraza, Irradiation-growth of zirconium-base alloys: Part i, Journal of Nuclear Materials 73 (2) (1978) 151–168.

[9] V. Shishov, A. V. Nikulina, V. A. Markelov, M. M. Peregud, A. V. Kozlov, S. A. Averin, S. A. Kolbenkov, A. E. Novoselov, Influence of neutron irradiation on dislocation structure and phase composition of zr-base alloys, in: Zirconium in the Nuclear Industry: Eleventh International Symposium, ASTM International, 1996, pp. 603–622.

[10] C. Woo, U. Gösele, Dislocation bias in an anisotropic diffusive medium and irradiation growth, Journal of Nuclear Materials 119 (2-3) (1983) 219–228.

[11] C. H. Woo, Theory of irradiation deformation in non-cubic metals: Effects of anisotropic diffusion, Journal of Nuclear Materials 159 (1988) 237–256. doi:10.1016/0022-3115(88)90096-7.

[12] R. Holt, C. Woo, C. Chow, Production bias—a potential driving force for irradiation growth, Journal of Nuclear Materials 205 (1993) 293–300.

[13] F. Christien, A. Barbu, Cluster Dynamics modelling of irradiation growth of zirconium single crystals, Journal of Nuclear Materials 393 (1) (2009) 153–161. doi:10.1016/j.jnucmat.2009.05.016.

[14] S. I. Choi, G.-G. Lee, J. Kwon, J. H. Kim, Modeling of sink-induced irradiation growth of single-crystal and polycrystal zirconiums in nuclear reactors, Journal of Nuclear Materials 468 (2016) 56–70. doi:10.1016/j.jnucmat.2015.11.014.

[15] A. V. Barashev, S. I. Golubov, R. E. Stoller, Theoretical investigation of microstructure evolution and deformation of zirconium under neutron irradiation, Journal of Nuclear Materials 461 (2015) 85–94. doi:10.1016/j.jnucmat.2015.02.001.

[16] S. Wooding, L. Howe, F. Gao, A. Calder, D. Bacon, A molecular dynamics study of high-energy displacement cascades in α-zirconium, Journal of Nuclear Materials 254 (2-3) (1998) 191–204.

[17] A. Jostsons, P. Kelly, R. Blake, K. Farrell, Neutron irradiation-induced defect structures in zirconium, in: Effects of radiation on structural materials, ASTM International, 1979, p. 46.

[18] D. O. Northwood, R. W. Gilbert, L. E. Bahen, P. M. Kelly, R. G. Blake, A. Jostsons, P. K. Madden, D. Faulkner, W. Bell, R. B. Adamson, Characterization of neutron irradiation damage in zirconium alloys — an international "round-robin" experiment, Journal of Nuclear Materials 79 (2) (1979) 379–394. doi:10.1016/0022-3115(79)90103-X.

[19] M. Griffiths, Microstructure evolution in hcp metals during irradiation, Philosophical Magazine A 63 (5) (1991) 835–847.

[20] M. Griffiths, Evolution of microstructure in hcp metals during irradiation, Journal of Nuclear Materials 205 (1993) 225–241.

[21] C. Ball, The contribution of the intrinsic anisotropy of point defect diffusion rates to irradiation growth of zirconium, Journal of Nuclear Materials 101 (1-2) (1981) 147–149.

[22] M. Christensen, W. Wolf, C. Freeman, E. Wimmer, R. B. Adamson, M. Griffiths, E. V. Mader, Vacancy loops in Breakaway Irradiation Growth of zirconium: Insight from atomistic simulations, Journal of Nuclear Materials 529 (2020) 151946. doi:10.1016/j.jnucmat.2019.151946.

[23] J. L. Katz, H. Wiedersich, Nucleation of voids in materials supersaturated with vacancies and interstitials, The Journal of Chemical Physics 55 (3) (1971) 1414–1425.

[24] A. Brailsford, R. Bullough, The rate theory of swelling due to void growth in irradiated metals, Journal of Nuclear Materials 44 (2) (1972) 121–135.

[25] L. K. Mansur, Void swelling in metals and alloys under irradiation: an assessment of the theory, Nuclear Technology 40 (1) (1978) 5–34.

[26] R. E. Voskoboinikov, Y. N. Osetsky, D. J. Bacon, Atomic-scale simulation of defect cluster formation in high-energy displacement cascades in zirconium, in: Effects of Radiation on Materials: 22nd Symposium, ASTM International, 2006, pp. 299–313.

[27] N. de Diego, Y. N. Osetsky, D. J. Bacon, Mobility of interstitial clusters in alpha-zirconium, Metallurgical and Materials Transactions A 33 (13) (2002) 783–789. doi:10.1007/s11661-002-1008-2.

[28] M. Makin, A. Whapham, F. Minter, The formation of dislocation loops in copper during neutron irradiation, Philosophical Magazine 7 (74) (1962) 285–299.

[29] J. Marian, V. V. Bulatov, Stochastic cluster dynamics method for simulations of multispecies irradiation damage accumulation, Journal of Nuclear Materials 415 (1) (2011) 84–95. doi:10.1016/j.jnucmat.2011.05.045.

[30] A. Y. Dunn, L. Capolungo, E. Martinez, M. Cherkaoui, Spatially resolved stochastic cluster dynamics for radiation damage evolution

in nanostructured metals, Journal of Nuclear Materials 443 (1) (2013) 128–139. doi:10.1016/j.jnucmat.2013.07.009.

[31] F. Christien, A. Barbu, Effect of self-interstitial diffusion anisotropy in electron-irradiated zirconium: A cluster dynamics modeling, Journal of Nuclear Materials 346 (2) (2005) 272–281. doi:10.1016/j.jnucmat.2005.06.024.

[32] S. Golubov, A. Barashev, R. Stoller, Mean field reaction rate theory, Encyclopedia of Comprehensive Nuclear Materials (2012) 357–391.

[33] S. Golubov, A. Barashev, R. Stoller, B. Singh, Breakthrough in Understanding Radiation Growth of Zirconium, ASTM Special Technical Publication 1543 (2015) 729–758. doi:10.1520/STP154320130043.

[34] J. Horvath, F. Dyment, H. Mehrer, Anomalous self-diffusion in a single crystal of α-zirconium, Journal of Nuclear Materials 126 (3) (1984) 206–214.

[35] N. Ghoniem, S. Sharafat, A numerical solution to the fokker-planck equation describing the evolution of the interstitial loop microstructure during irradiation, Journal of Nuclear Materials 92 (1) (1980) 121–135.

[36] N. Ghoniem, Stochastic theory of diffusional planar-atomic clustering and its application to dislocation loops, Physical Review B 39 (16) (1989) 11810.

[37] N. M. Ghoniem, D. D. Cho, The Simultaneous Clustering of Point Defects during Irradiation, Physica Status Solidi (A) 54 (1) (1979) 171–178. doi:10.1002/pssa.2210540122.

[38] N. De Diego, Y. N. Osetsky, D. Bacon, Structure and properties of vacancy and interstitial clusters in α-zirconium, Journal of Nuclear Materials 374 (1-2) (2008) 87–94.

[39] B. Christiaen, C. Domain, L. Thuinet, A. Ambard, A. Legris, A new scenario for c vacancy loop formation in zirconium based on atomic-scale modeling, Acta Materialia 179 (2019) 93–106. doi:10.1016/j.actamat.2019.07.030.

[40] S. MacEwen, G. Carpenter, Calculations of irradiation growth in zirconium, Journal of Nuclear Materials 90 (1-3) (1980) 108–132.

[41] M. Griffiths, M. H. Loretto, R. E. Smallman, Electron damage in zirconium: II. Nucleation and growth of c-component loops, Journal of Nuclear Materials 115 (2) (1983) 323–330. doi:10.1016/0022-3115(83)90323-9.

[42] G. Carpenter, R. Murgatroyd, A. Rogerson, J. Watters, Irradiation growth of zirconium single crystals, Journal of Nuclear Materials 101 (1-2) (1981) 28–37.

[43] A. Rogerson, R. H. Zee, High fluence irradiation growth in single crystal zirconium at 553 K, Journal of Nuclear Materials 151 (1) (1987) 81–83. doi:10.1016/0022-3115(87)90059-6.

[44] A. Rogerson, Irradiation growth in zirconium and its alloys, Journal of Nuclear Materials 159 (1988) 43–61. doi:10.1016/0022-3115(88)90084-0.

[45] A. G. Mikhin, Y. N. Osetsky, V. G. Kapinos, On the anisotropic migration of point defects in h.c.p. zirconium, Philosophical Magazine A 70 (1) (1994) 25–33. doi:10.1080/01418619408242534.

[46] S. MacEwen, R. Zee, R. Birtcher, C. Abkomeit, Point defect production and annihilation in neutron-irradiated zirconium, Journal of Nuclear Materials 123 (1-3) (1984) 1036–1040.

[47] A. Jostsons, P. Kelly, R. Blake, The nature of dislocation loops in neutron irradiated zirconium, Journal of Nuclear Materials 66 (3) (1977) 236–256.

[48] R. Gilbert, K. Farrell, C. Coleman, Damage structure in zirconium alloys neutron irradiated at 573 to 923 k, Journal of Nuclear Materials 84 (1-2) (1979) 137–148.

[49] Radiation Damage to Zirconium and Its Alloys, in: J. Koutský, J. Kočik (Eds.), Materials Science Monographs, Vol. 79 of Radiation Damage of Structural Materials, Elsevier, 1994, pp. 236–263. doi:10.1016/B978-0-444-98708-2.50012-X.

[50] A. Jostsons, R. Blake, J. Napier, P. Kelly, K. Farrell, Faulted loops in neutron-irradiated zirconium, Journal of Nuclear Materials 68 (3) (1977) 267–276.

[51] C. Hellio, C. H. de Novion, L. Boulanger, Influence of alloying elements on the dislocation loops created by Zr+ ion or by electron irradiation in α-zirconium, Journal of Nuclear Materials 159 (1988) 368–378. doi:10.1016/0022-3115(88)90103-1.

[52] D. Northwood, Irradiation damage in zirconium and its alloys, Atomic Energy Review 15 (4) (1977) 547–610.

[53] L. F. Shampine, M. W. Reichelt, The matlab ode suite, SIAM Journal on Scientific Computing 18 (1) (1997) 1–22.

[54] G. Carpenter, R. Zee, A. Rogerson, Irradiation growth of zirconium single crystals: A review, Journal of Nuclear Materials 159 (1988) 86–100.

[55] M. Griffiths, A review of microstructure evolution in zirconium alloys during irradiation, Journal of Nuclear Materials 159 (1988) 190–218.

[56] V. Fidleris, R. Tucker, R. Adamson, An overview of microstructural and experimental factors that affect the irradiation growth behavior of zirconium alloys, in: Zirconium in the Nuclear Industry, ASTM International, 1987, pp. 49–85.

[57] D. Bacon, F. Gao, Y. N. Osetsky, Computer simulation of displacement cascades and the defects they generate in metals, Nuclear Instruments and Methods in Physics Research Section B: Beam Interactions with Materials and Atoms 153 (1-4) (1999) 87–98.

[58] D. J. Bacon, Y. N. Osetsky, R. Stoller, R. E. Voskoboinikov, Md description of damage production in displacement cascades in copper and α-iron, Journal of Nuclear Materials 323 (2-3) (2003) 152–162.

[59] C. Arévalo, M. Caturla, J. Perlado, Temperature dependence of damage accumulation in α-zirconium, Journal of nuclear materials 367 (2007) 338–343.

[60] D. Kulikov, M. Hou, Vacancy dislocation loops in zirconium and their interaction with self-interstitial atoms, Journal of Nuclear Materials 342 (1-3) (2005) 131–140.

[61] R. Voskoboinikov, Y. N. Osetsky, D. Bacon, Identification and morphology of point defect clusters created in displacement cascades in α-zirconium, Nuclear Instruments and Methods in Physics Research Section B: Beam Interactions with Materials and Atoms 242 (1-2) (2006) 530–533.

[62] C. Dai, Atomistic simulations of irradiation-induced dislocation loops in zirconium alloys, Ph.D. thesis, Queen's University (2018).

[63] C. Varvenne, O. Mackain, E. Clouet, Vacancy clustering in zirconium: An atomic-scale study, Acta Materialia 78 (2014) 65–77.